

Lattice Boltzmann simulations of the bead-spring microswimmer with a responsive stroke—from an individual to swarms

This content has been downloaded from IOPscience. Please scroll down to see the full text.

2017 J. Phys.: Condens. Matter 29 124001

(<http://iopscience.iop.org/0953-8984/29/12/124001>)

View [the table of contents for this issue](#), or go to the [journal homepage](#) for more

Download details:

IP Address: 193.198.162.14

This content was downloaded on 14/03/2017 at 09:03

Please note that [terms and conditions apply](#).

You may also be interested in:

[Hydrodynamics of linked sphere model swimmers](#)

G P Alexander, C M Pooley and J M Yeomans

[A three-sphere swimmer for flagellar synchronization](#)

Katja Polotzek and Benjamin M Friedrich

[Physics of microswimmers—single particle motion and collective behavior: a review](#)

J Elgeti, R G Winkler and G Gompper

[The hydrodynamics of swimming microorganisms](#)

Eric Lauga and Thomas R Powers

[Confined swimming of bio-inspired microrobots in rectangular channels](#)

Fatma Zeynep Temel and Serhat Yesilyurt

[Phase-dependent forcing and synchronization in the three-sphere model of Chlamydomonas](#)

Rachel R Bennett and Ramin Golestanian

[Dynamics of confined suspensions of swimming particles](#)

Juan P Hernandez-Ortiz, Patrick T Underhill and Michael D Graham

[Emergent behavior in active colloids](#)

Andreas Zöttl and Holger Stark

[Can the self-propulsion of anisotropic microswimmers be described by using forces and torques?](#)

Borge ten Hagen, Raphael Wittkowski, Daisuke Takagi et al.

Lattice Boltzmann simulations of the bead-spring microswimmer with a responsive stroke—from an individual to swarms

Kristina Pickl^{1,2,6}, Jayant Pande^{2,3,6}, Harald Köstler¹, Ulrich Rüde^{1,5}
and Ana-Sunčana Smith^{2,3,4,7,8}

¹ Chair for System Simulation, Friedrich-Alexander University Erlangen-Nürnberg, Cauerstraße 11, 91058 Erlangen, Germany

² Cluster of Excellence: EAM, Friedrich-Alexander University Erlangen-Nürnberg, Nägelsbachstraße 49b, 91054 Erlangen, Germany

³ PULS Group, Department of Physics, Friedrich-Alexander University Erlangen-Nürnberg, Nägelsbachstraße 49b, 91054 Erlangen, Germany

⁴ Division of Physical Chemistry, Ruđer Bošković Institute, Bijenička cesta 54, Zagreb, Croatia

⁵ CERFACS (Centre Européen de Recherche et de Formation Avancée en Calcul Scientifique), 42 Avenue Gaspard Coriolis, 31057 Toulouse Cedex 1, France

E-mail: smith@physik.fau.de

Received 14 October 2016, revised 31 December 2016

Accepted for publication 18 January 2017

Published 8 February 2017




CrossMark

Abstract

Propulsion at low Reynolds numbers is often studied by defining artificial microswimmers which exhibit a particular stroke. The disadvantage of such an approach is that the stroke does not adjust to the environment, in particular the fluid flow, which can diminish the effect of hydrodynamic interactions. To overcome this limitation, we simulate a microswimmer consisting of three beads connected by springs and dampers, using the self-developed WALBERLA and *pe* framework based on the lattice Boltzmann method and the discrete element method. In our approach, the swimming stroke of a swimmer emerges as a balance of the drag, the driving and the elastic internal forces. We validate the simulations by comparing the obtained swimming velocity to the velocity found analytically using a perturbative method where the bead oscillations are taken to be small. Including higher-order terms in the hydrodynamic interactions between the beads improves the agreement to the simulations in parts of the parameter space. Encouraged by the agreement between the theory and the simulations and aided by the massively parallel capabilities of the WALBERLA-*pe* framework, we simulate more than ten thousand such swimmers together, thus presenting the first fully resolved simulations of large swarms with active responsive components.

Keywords: microswimming, three-sphere swimmer, lattice Boltzmann method, many-swimmer swarms, perturbation theory, Rotne–Prager theory

 Supplementary material for this article is available [online](#)

(Some figures may appear in colour only in the online journal)

⁶ These authors contributed equally to this work.

⁷ Author to whom any correspondence should be addressed.

⁸ This article belongs to the [special issue: Emerging Leaders](#), which features invited work from the best early-career researchers working within the scope of *Journal of Physics: Condensed Matter*. This project is part of the *Journal of Physics series'* 50th anniversary celebrations in 2017. Ana-Sunčana Smith was selected by the Editorial Board of *Journal of Physics: Condensed Matter* as an Emerging Leader.

1. Introduction

In the last few years a lot of research activity has focussed on studying microlocomotion through analytical, experimental and numerical means (for comprehensive reviews see [1, 2]). Much of this focus has been on the collective movement of micro-organisms, since in nature these organisms tend to live

and move together in huge clusters numbering up to millions of individuals [3–9]. The interactions amongst the various individuals impart new biological and physical features to their motion and their experience of their surroundings that are missing in the case of isolated swimmers.

A customary approach to model mechanical microswimmers theoretically is to assume that the swimming stroke of the model swimmer is known or is imposed [10–16]. With this approach, the hydrodynamic features of the motion are in essence smoothed over and the problem becomes a purely geometrical one, which simplifies both the numerical simulation as well as the analysis of the motion considerably. Especially for the study of swimmer swarms, such a simplification is often crucial for reducing the computational complexity of the setup. However, the biggest advantage of this approach—the reduced dependence of the swimmer on the fluid flow—is also its biggest weakness, as it robs the system of a full reliance on the hydrodynamic forces, suppressing for instance the hydrodynamic interactions between different parts of the swimmer or between different swimmers in large populations.

The alternative approach is to specify not the swimming stroke itself but the forces which drive the swimming motion. The swimming stroke then emerges in response to the various forces acting on the system, which are typically the driving forces, the hydrodynamic forces, and the internal forces of tension or elasticity in the swimmer connecting the different body parts. Such an approach has been adopted in studies of the motion of *Chlamydomonas reinhardtii* or similar swimmers [17, 18], of a deformable infinite slab [19], and of the three-sphere swimmer [20, 21]. This approach has however not been employed so far in the service of simulating large swarms of swimmers, owing to the formidable computational costs it entails.

In this paper we use the latter, force-based, approach in both simulating and theoretically analyzing the motion of individuals as well as swarms of the bead-spring swimmer [21]. This swimmer is based on the three-sphere model introduced by Najafi and Golestanian [15] but differs from it in precisely the way described above, i.e. in its imposition of the forces driving the motion instead of the stroke of swimming, with the latter adapting dynamically to the former. Another difference is that in our swimmer the different beads are connected by harmonic springs and dampers. Our simulations are run by a combined framework of WALBERLA [22], which is a lattice Boltzmann fluid solver, and *pe*, which is a discrete element method-based physics engine, with both these systems optimized for the simulation of our bead-spring swimmer on hundreds of thousands of parallel processes [23].

We begin with a comparison of the simulations of an isolated bead-spring swimmer to analytical calculations. In previous work [21] we have employed a perturbative theory to calculate the swimmer velocity, where the variable of perturbation is the displacement of the beads from their equilibrium positions [20]. Here we extend this calculation by taking higher-order terms in the hydrodynamic interactions between the beads into account by using the Rotne–Prager tensor. We show that the velocities obtained in the simulations compare well to the theoretical values, and, at low swimming cycle periods, the higher-order theory shows better agreement with the simulations. The single-swimmer study helps us identify

the parameters which lead to relatively fast swimming, and we employ one such set of parameters to simulate swarms containing more than ten thousand individual swimmers, again with the forces and the geometries of the swimmers described completely. The massively parallel capabilities of our WALBERLA-*pe* simulation framework are here crucial, since they lead to, in our knowledge, the first simulations of swarms where the swimmers and the forces on them are fully resolved, without taking recourse to effective strokes or velocity fields [24–27]. We find that a highly symmetric arrangement of the swimmers is stable over the simulated time, but small differences in the initial separation between the swimmers result in continuously growing deviations as a result of strong asymmetric hydrodynamic interactions.

2. Basic swimmer model

Our basic swimmer, which shall be used throughout this paper in individual or grouped arrangements, consists of three rigid spherical beads of equal radii λ connected by two linear springs of equal stiffness constants k and mean rest lengths l . The model assumes the far-field limit, that is the limit $\lambda \ll l$. In this limit, beads of any shape different from spheres can equally well be used by defining λ as the friction coefficient of the shape scaled by a factor of $6\pi\eta$ [21]. In the following, we will consequently call λ the reduced friction coefficient of a bead.

In the simulations, we include additionally angular springs of high stiffness constants to ensure that the three beads remain collinear [23]. These angular springs are excluded from the theoretical model under the assumption that the motion of an isolated swimmer occurs strictly in a straight line. Time-irreversibility in the stroke, as required by the Scallop theorem for net propulsion at zero Reynolds number [28], is achieved via the sinusoidal driving forces

$$\begin{aligned} \mathbf{F}_1^d(t) &= A \sin(\omega t) \hat{\mathbf{x}}, \\ \mathbf{F}_2^d(t) &= -\mathbf{F}_1^d(t) - \mathbf{F}_3^d(t), \text{ and} \\ \mathbf{F}_3^d(t) &= B \sin(\omega t + \alpha) \hat{\mathbf{x}} \text{ with } \alpha \in [-\pi, \pi], \end{aligned} \quad (2.1)$$

that are applied to the centers of mass of the beads along the x -axis which is also the direction along which all swimmers are aligned at the beginning of each simulation. Such a force protocol may be realized if the beads are acted upon by external fields. The parameters A and B denote the amplitudes of the sinusoidal forces, ω is the force frequency, α is the relative phase shift in the forces and t is the instantaneous time. The sum of the three driving forces is always kept zero, so that the criterion of force neutrality is satisfied.

Due to the driving forces, the positions $\mathbf{R}_i(t)$ of the beads change, resulting in deformation of the springs and consequent spring forces $\mathbf{F}_i^s(t)$ given by

$$\begin{aligned} \mathbf{F}_i^s(t) &= \sum_{j \neq i}^3 \mathbf{G}(\mathbf{R}_i(t) - \mathbf{R}_j(t)), \text{ with} \\ \mathbf{G}(\mathbf{R}_i(t) - \mathbf{R}_j(t)) &= -k \left(\frac{\mathbf{R}_i(t) - \mathbf{R}_j(t)}{|\mathbf{R}_i(t) - \mathbf{R}_j(t)|} \right) (|\mathbf{R}_i(t) - \mathbf{R}_j(t)| - l) \end{aligned} \quad (2.2)$$

if i and j denote neighboring beads, and $\mathbf{G}(\mathbf{R}_i(t) - \mathbf{R}_j(t)) = \mathbf{0}$ otherwise. As the beads oscillate, the trailing and leading arms of the swimmer perform sinusoidal motion with oscillation amplitudes d_1 and d_2 , respectively (figure 1).

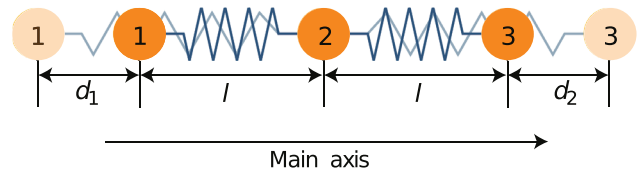


Figure 1. The bead-spring swimmer.

3. Simulation framework

The simulation system that we employ consists of two parts, the parallel lattice Boltzmann framework WALBERLA [22, 29, 30] for simulating the fluid, and the rigid body engine *pe* based on the discrete element method [31] for the beads within it.

The WALBERLA fluid solver uses a D3Q19 model [32] for three-dimensional space discretization employing 19 particle distribution functions (PDFs) per lattice site. For the collision operator, Ginzburg’s two-relaxation time model [33] is applied, which splits the PDFs, the used incompressible equilibrium distribution function, and the relaxation parameter into symmetric and antisymmetric parts. For the simulations, the best accuracy at the solid walls is achieved with the symmetric relaxation parameter set to $1/\tau$ and the antisymmetric one set to $8(2 - 1/\tau)/(8 - 1/\tau)$ [33], where τ denotes the relaxation time. The software utilizes the message passing interface (MPI) and is optimized for scalable and efficient execution on the fastest supercomputers available [34].

The physics engine *pe* [31] handles the dynamics of the rigid body parts of the swimmer using Newton’s equations of motion, and includes mechanisms for resolving frictional rigid body collisions and modelling external forces like gravity or the sinusoidal forces driving the swimmer. The algorithm is augmented with an MPI communication strategy that can handle general pairwise spring-damper systems [35]. To avoid problems resulting from non-local communication among processes resulting from extended springs, communication is restricted to those pairs of processes on which objects interact. Global communication is avoided since it might lead to a deterioration of parallel performance and scalability on modern supercomputers [23], a particularly important concern for the simulation of swarms.

The interactions between the swimmer and the fluid, as well as between different bodies within the swimmer, are modelled by a four-way coupling scheme [23, 35, 36]. The rigid bodies of the swimmer overlap with the cells of the LBM grid and are marked as obstacles within the fluid resulting in a staircase approximation of the rigid bodies. Those that interface to the fluid are specified to have a moving boundary condition [37–39]. The fluid couples to a rigid body via the momentum exchange method [37, 38, 40] that takes into account the instantaneously acting hydrodynamic forces from the fluid on the rigid body.

4. Study of an individual swimmer

We first investigate the case of a single swimmer swimming far away from any boundaries or from any other swimmers. In response to the driving forces, the swimming stroke induced is sinusoidal, and can be expressed as

$$\begin{aligned} L_1(t) &= l + d_1 \cos(\omega t + \delta_1), \\ L_2(t) &= l + d_2 \cos(\omega t + \delta_2), \end{aligned} \quad (4.1)$$

where L_i is the instantaneous length of the i th arm, and d_i and δ_i are the amplitude and the phase of its oscillation. Once this form of the swimming stroke is adopted, and the conditions of no fluid slip, large bead separations (justifying the use of the Oseen tensor in specifying the inter-bead hydrodynamic interactions) and small arm-length oscillations are assumed, then the swimmer’s velocity can be written as [41]

$$\mathbf{v}_S^O = G d_1 d_2 \omega \sin(\delta_1 - \delta_2). \quad (4.2)$$

Here \mathbf{v}_S^O is the swimming velocity (with the subscript ‘S’ referring to the stroke-based nature of its calculation and the superscript ‘O’ to the use of the Oseen tensor), and G is a geometrical constant which for equal bead reduced friction coefficients λ and equal mean arm-lengths l is given by $G = 7\lambda/(24l^2)$.

The above is the stroke-centric calculation of the swimming velocity. In previous work [21], we have calculated the velocity of the swimmer in the force-centric picture by considering the effect on each bead of the different forces it faces, these being the spring forces, the driving forces and the hydrodynamic forces. For small driving forces, the oscillations of the beads are small too, and we obtain a coupled system of ordinary differential equations for the bead positions as functions of time, due to the linear velocity-force relationship in Stokes flow mediated by the Oseen tensor [42]. We solve this system in a perturbative manner (as in [20]) with the oscillation of the swimmer arms being the variable of perturbation. Calculation of the velocity to the second order in the armlength oscillation amplitudes—since the zeroth and the first orders turn out not to contribute, due to the sinusoidal nature of the driving and the armlength oscillations which integrate to zero over a cycle—leads finally to the following expression (in the notation employed in this paper) [21],

$$\mathbf{v}_F^O = \frac{7\lambda\omega [AB(k^2 + 12\pi^2\eta^2\omega^2\lambda^2) \sin \alpha + 2(A^2 - B^2)\pi\eta\omega k\lambda]}{24l^2(k^2 + 4\pi^2\eta^2\omega^2\lambda^2)(k^2 + 36\pi^2\eta^2\omega^2\lambda^2)} \hat{\mathbf{x}}. \quad (4.3)$$

Here \mathbf{v}_F^O denotes the swimming velocity calculated using the forces (hence the subscript ‘F’) acting upon the swimmer and with the superscript ‘O’ again marking the use of the Oseen tensor. The dynamic viscosity of the fluid is η . The above calculation assumes that there is no slip between the beads and the fluid, and that the distances between the beads are much larger than their radii (that is $l/\lambda \gg 1$), and the results are correct only to the lowest order in λ/l .

The two approaches of finding the swimming velocity—i.e. assuming known driving forces and known strokes—may be reconciled by determining the various stroke parameters for the assumed force protocol, and then using the now-known strokes to find the velocity as in (4.2). The amplitudes of oscillation of the two arms are found to be [21]

$$d_1 = \sqrt{\frac{A^2 k^2 + 4\pi^2 \eta^2 \omega^2 \lambda^2 (4A^2 + B^2 + 4AB \cos \alpha) - 4AB\pi\eta\omega k \lambda \sin \alpha}{k^4 + 40\pi^2 \eta^2 \omega^2 k^2 \lambda^2 + 144\pi^4 \eta^4 \omega^4 \lambda^4}}, \text{ and} \quad (4.4)$$

$$d_2 = \sqrt{\frac{B^2 k^2 + 4\pi^2 \eta^2 \omega^2 \lambda^2 (A^2 + 4B^2 + 4AB \cos \alpha) + 4AB\pi\eta\omega k \lambda \sin \alpha}{k^4 + 40\pi^2 \eta^2 \omega^2 k^2 \lambda^2 + 144\pi^4 \eta^4 \omega^4 \lambda^4}}. \quad (4.5)$$

Defining β as the stroke phase shift $\beta = \delta_1 - \delta_2$, its sinusoidal function is given by

$$\sin \beta = \frac{N}{D}, \text{ where} \quad (4.6)$$

$$N = 2(A^2 - B^2)\pi\eta\omega k r + AB(k^2 + 12\pi^2 \eta^2 \omega^2 r^2) \sin \alpha, \text{ and} \quad (4.7)$$

$$D = \{A^2 B^2 k^4 + 4\pi\eta\omega r[\pi\eta\omega k^2 r(A^4 + 6A^2 B^2 + B^4) + 4\pi^3 \eta^3 \omega^3 r^3(4A^4 + 25A^2 B^2 + 4B^4) + 4AB\pi\eta\omega r \cos \alpha(A^2 + B^2)(k^2 + 20\pi^2 \eta^2 \omega^2 r^2) + 2A^2 B^2 \pi\eta\omega r(k^2 + 16\pi^2 \eta^2 \omega^2 r^2) \cos(2\alpha) + ABk \sin \alpha(A^2 - B^2)(k^2 + 12\pi^2 \eta^2 \omega^2 r^2)]\}^{1/2}. \quad (4.8)$$

The stroke- and the force-based velocity expressions are then found to be related as

$$\mathbf{v}_S^O = \frac{7(4l - 3\lambda)(4l - 7\lambda)}{4l(28l - 45\lambda)} \mathbf{v}_F^O. \quad (4.9)$$

To the lowest order in λ/l , the two velocities agree.

4.1. Velocity calculation to higher order in hydrodynamic interaction

We now extend the above calculation in order to take higher-order terms in the hydrodynamic interactions amongst the beads into account. Including these terms loosens the requirement on the ratio l/λ to be large, and is beneficial for comparison with our simulations where this ratio l/λ equals 5. For the calculation, we employ the Rotne–Prager matrix [43] which gives the hydrodynamic interaction terms to one order higher than the Oseen approximation. This involves the use of the method of reflections [44]. Section 5.10 in [45] provides the Rotne–Prager matrix for a suspension of spheres of equal radii. We here present the derivation of the matrix for beads with possibly unequal reduced friction coefficients λ_i (which, for spherical beads, equal their radii). Note that the ‘higher-order’ label for this calculation refers not to the perturbation scheme used—since the velocity is again calculated to the second order in the armlength oscillation amplitudes, as in section 4—but to the precision of the terms specifying the hydrodynamic interaction amongst the beads.

We start with the flow field induced in an initially motionless fluid by a bead of reduced friction coefficient λ_j and velocity \mathbf{v}_j

positioned instantaneously at the origin of the coordinate system. This flow field $\mathbf{u}(\mathbf{r})$ at the point \mathbf{r} in the fluid is given by [45]

$$\mathbf{u}(\mathbf{r}) = \left\{ \frac{3}{4} \frac{\lambda_j}{|\mathbf{r}|} \left(\mathbb{I} + \frac{\mathbf{r}\mathbf{r}}{|\mathbf{r}|^2} \right) + \frac{1}{4} \left(\frac{\lambda_j}{|\mathbf{r}|} \right)^3 \left(\mathbb{I} - 3 \frac{\mathbf{r}\mathbf{r}}{|\mathbf{r}|^2} \right) \right\} \cdot \mathbf{v}_j. \quad (4.10)$$

For our assembly of beads, the flow field induced by each bead then affects the motion of the other beads. The change in the other beads’ velocities is given by Faxén’s theorem for translational motion [46], which states that the velocity \mathbf{v}_i acquired by a sphere of radius a_i immersed at the position \mathbf{r}_i in a fluid with a flow velocity field $\mathbf{u}(\mathbf{r})$ is given by

$$\mathbf{v}_i = \frac{-1}{6\pi\eta a_i} \mathbf{F}_i^h + \mathbf{u}(\mathbf{r}_i) + \frac{1}{6} a_i^2 \nabla_i^2 \mathbf{u}(\mathbf{r}_i), \quad (4.11)$$

where \mathbf{F}_i^h is the hydrodynamic drag force on the sphere in question.

In our case, clearly, the velocity \mathbf{v}_i of the i th bead is affected by the fluid flow $\mathbf{u}(\mathbf{r})$ induced by the j th bead swimming with the velocity \mathbf{v}_j at the instantaneous position \mathbf{r}_j in the fluid. Since the velocity of the j th bead in the absence of any other bead is given by the Stokes drag law

$$\mathbf{v}_j = \frac{-1}{6\pi\eta\lambda_j} \mathbf{F}_j^h, \quad (4.12)$$

therefore, combining equations (4.10)–(4.12) and simplifying the expressions (see Appendix for details), we find the velocity of the i th bead in terms of the drag forces on the i th and the j th beads to be

$$\mathbf{v}_i = \frac{-1}{6\pi\eta\lambda_i} \mathbf{F}_i^h - \sum_{j \neq i} \left[\frac{1}{8\pi\eta r_{ij}} (\mathbb{I} + \hat{\mathbf{r}}_{ij} \hat{\mathbf{r}}_{ij}) + \frac{1}{24\pi\eta} \frac{\lambda_j + \lambda_i}{r_{ij}^3} (\mathbb{I} - 3\hat{\mathbf{r}}_{ij} \hat{\mathbf{r}}_{ij}) \right] \cdot \mathbf{F}_j^h \quad (4.13)$$

$$\left(\text{where } \hat{\mathbf{r}}_{ij} \equiv \frac{(\mathbf{r}_i - \mathbf{r}_j)(\mathbf{r}_i - \mathbf{r}_j)}{|\mathbf{r}_i - \mathbf{r}_j|^2} \text{ and } r_{ij} \equiv |\mathbf{r}_i - \mathbf{r}_j| \right) \\ = \frac{-1}{6\pi\eta\lambda_i} \mathbf{F}_i^h - \sum_{j \neq i} [\mathbf{T}(\mathbf{r}_{ij}) + \mathbf{W}(\mathbf{r}_{ij})] \cdot \mathbf{F}_j^h, \quad (4.14)$$

where $\mathbf{T}(\mathbf{r}_{ij})$ and $\mathbf{W}(\mathbf{r}_{ij})$ denote respectively the first and the second terms in the summation in (4.13) (with $\mathbf{T}(\mathbf{r})$ being the Oseen tensor). The sum of these two terms, $\mathbf{T}(\mathbf{r}_{ij}) + \mathbf{W}(\mathbf{r}_{ij})$, is the Rotne–Prager matrix for an assembly of spherical beads of radii λ_i .

Using (4.14) we can write out in full the velocities of the three beads in our swimmer as

$$\mathbf{v}_1 = \frac{1}{6\pi\eta} \begin{pmatrix} 0 \\ 0 \\ \left[\frac{3}{2(L_1+L_2)} - \frac{\lambda_1^2 + \lambda_3^2}{2(L_1+L_2)^3} \right] F_3^{d+s} \end{pmatrix}, \quad (4.15)$$

$$\mathbf{v}_2 = \frac{1}{6\pi\eta} \begin{pmatrix} 0 \\ 0 \\ \left(\frac{3}{2L_1} - \frac{\lambda_1^2 + \lambda_2^2}{2L_1^3} \right) F_1^{d+s} + \frac{F_2^{d+s}}{\lambda_2} + \left(\frac{3}{2L_2} - \frac{\lambda_2^2 + \lambda_3^2}{2L_2^3} \right) F_3^{d+s} \end{pmatrix}, \text{ and} \quad (4.16)$$

$$\mathbf{v}_3 = \frac{1}{6\pi\eta} \begin{pmatrix} 0 \\ 0 \\ \left[\frac{3}{2(L_1+L_2)} - \frac{\lambda_1^2 + \lambda_3^2}{2(L_1+L_2)^3} \right] F_1^{d+s} + \left(\frac{3}{2L_2} - \frac{\lambda_2^2 + \lambda_3^2}{2L_2^3} \right) F_2^{d+s} + \frac{F_3^{d+s}}{\lambda_3} \end{pmatrix}. \quad (4.17)$$

Here F_i^{d+s} is shorthand for the magnitude of the sum of the spring and driving forces on the i th bead (i.e. $\mathbf{F}_i^s + \mathbf{F}_i^d$, with these forces given by equations (2.1) and (2.2)), which can replace the (negative of the) drag force on the bead since the spring, the driving and the drag forces on each bead always sum to zero. In equations (4.15)–(4.17) the time-dependence of the armlengths $L_i(t)$, the forces $F_i^{d+s}(t)$ and the velocities $\mathbf{v}_i(t)$ has been suppressed for brevity of expression.

From the velocities of the beads, the velocity of the swimmer \mathbf{v}_F^{RP} (where the superscript ‘RP’ in the swimmer velocity denotes the use of the Rotne–Prager matrix in finding the velocity within the force-based formulation) may be found by averaging $\mathbf{v}_i(t)$ over the three beads and over one cycle period, i.e.

$$\mathbf{v}_F^{\text{RP}} = \frac{\omega}{6\pi} \int_0^{2\pi/\omega} dt \sum_{i=1}^3 \mathbf{v}_i(t). \quad (4.18)$$

Equations (4.15)–(4.18) are the equations of motion for the system, differential in the bead positions $\mathbf{R}_i(t)$, which are related to the velocities $\mathbf{v}_i(t)$ as

$$\mathbf{v}_i(t) = \frac{d\mathbf{R}_i(t)}{dt} (i = 1, 2, 3), \quad (4.19)$$

and which enter into both the armlengths $L_i(t)$ and the forces $F_i^{d+s}(t)$ (the latter because the spring forces depend on the bead positions).

To solve this coupled system of differential equations, we adopt a perturbative approach following a method proposed in [20], wherein we assume that in the steady state the swimmer’s motion consists of a uniformly-moving equilibrium configuration with the three beads executing small sinusoidal oscillations around this configuration. In particular, the bead positions are assumed to be of the form

$$\mathbf{R}_i(t) = \mathbf{S}_{i0} + \boldsymbol{\xi}_i(t) + \mathbf{v}_F^{\text{RP}} t, \quad (4.20)$$

where $\boldsymbol{\xi}_i(t)$ denotes small sinusoidal oscillations around the equilibrium configuration \mathbf{S}_{i0} of the swimmer. We expand the functions of the relative bead positions ($\mathbf{R}_i(t) - \mathbf{R}_j(t)$) in equations (4.15)–(4.18) in terms of series of the variables $(\boldsymbol{\xi}_i(t) - \boldsymbol{\xi}_j(t))$ centred around the equilibrium configuration,

which can be taken to be the configuration at time $t = 0$. The different variables which depend on $(\mathbf{R}_i(t) - \mathbf{R}_j(t))$ are the functions $\mathbf{G}(\mathbf{R}_i(t) - \mathbf{R}_j(t))$ specifying the spring forces (from (2.2)) and the functions $\mathbf{T}(\mathbf{R}_i(t) - \mathbf{R}_j(t)) + \mathbf{W}(\mathbf{R}_i(t) - \mathbf{R}_j(t))$ defining the Rotne–Prager matrix for the system. To the first order in $(\boldsymbol{\xi}_i(t) - \boldsymbol{\xi}_j(t))$, these functions are expanded to

$$\begin{aligned} \mathbf{G}(\mathbf{R}_i(t) - \mathbf{R}_j(t)) &= \mathbf{G}(\mathbf{R}_i(0) - \mathbf{R}_j(0)) + \left. \frac{\partial \mathbf{G}(\mathbf{R}_i(t) - \mathbf{R}_j(t))}{\partial \mathbf{R}_i(t)} \right|_{t=0} \cdot (\boldsymbol{\xi}_i(t) - \boldsymbol{\xi}_j(t)) \\ &= \mathbf{H}_{ij} \cdot (\boldsymbol{\xi}_i(t) - \boldsymbol{\xi}_j(t)), \text{ with } \mathbf{H}_{ij} = \left. \frac{\partial \mathbf{G}(\mathbf{R}_i(t) - \mathbf{R}_j(t))}{\partial \mathbf{R}_i(t)} \right|_{t=0}, \end{aligned} \quad (4.21)$$

$$\begin{aligned} \mathbf{T}(\mathbf{R}_i(t) - \mathbf{R}_j(t)) &= \mathbf{T}(\mathbf{R}_i(0) - \mathbf{R}_j(0)) + \left. \frac{\partial \mathbf{T}(\mathbf{R}_i(t) - \mathbf{R}_j(t))}{\partial \mathbf{R}_i(t)} \right|_{t=0} \cdot (\boldsymbol{\xi}_i(t) - \boldsymbol{\xi}_j(t)) \\ &= \mathbf{T}_{ij} + \mathbf{P}_{ij} \cdot (\boldsymbol{\xi}_i(t) - \boldsymbol{\xi}_j(t)), \\ \text{with } \mathbf{T}_{ij} &= \mathbf{T}(\mathbf{R}_i(0) - \mathbf{R}_j(0)) \text{ and } \mathbf{P}_{ij} = \left. \frac{\partial \mathbf{T}(\mathbf{R}_i(t) - \mathbf{R}_j(t))}{\partial \mathbf{R}_i(t)} \right|_{t=0}, \end{aligned} \quad (4.22)$$

and a similar expansion as (4.22) for $\mathbf{W}(\mathbf{R}_i(t) - \mathbf{R}_j(t))$, with $\mathbf{T}(\mathbf{R}_i(t) - \mathbf{R}_j(t))$, \mathbf{T}_{ij} and \mathbf{P}_{ij} in (4.22) being replaced respectively by $\mathbf{W}(\mathbf{R}_i(t) - \mathbf{R}_j(t))$, \mathbf{W}_{ij} and \mathbf{Q}_{ij} .

Using the above expansions, equations (4.15)–(4.18) can be solved to successive orders in $\boldsymbol{\xi}_i$. We find that the lowest order in $\boldsymbol{\xi}_i$ turns out to be 2, because the forces as well as the displacements are of a sinusoidal form and sinusoidal functions are orthonormal. The final expression obtained for the velocity is accurate to the lowest order in $\boldsymbol{\xi}_i$ and the second lowest order in λ/l , the latter due to the use of the Rotne–Prager tensor instead of the Oseen tensor in describing the hydrodynamic interactions amongst the beads. This velocity expression is rather long, and for simplicity we here state it only for the case of equal driving force amplitudes $A = B$, in which case it reads

$$\mathbf{v}_F^{\text{RP}} = \frac{A^2 \omega \lambda (28l - 45\lambda) [(2l - 5\lambda)k^2 + 24\pi^2 \eta^2 \omega^2 \lambda^2 l]}{192l^3 [(l - 5\lambda)k^4 + 4\pi^2 \eta^2 \omega^2 \lambda^2 (8l - 33\lambda)k^2 + 144\pi^4 \eta^4 \omega^4 \lambda^4 l]} \hat{\mathbf{x}}. \quad (4.23)$$

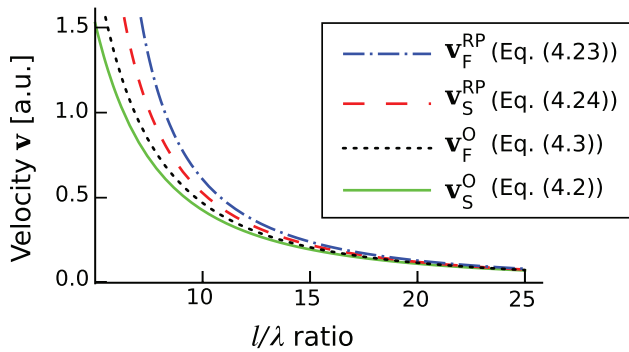


Figure 2. Comparison of theoretically calculated velocities of a swimmer from both force- and stroke-based approaches, as the bead separation-to-radius ratio (l/λ) decreases.

Following the above procedure, we can also find the corresponding expression in the stroke-based formulation. In terms of the swimming stroke specified in (4.1), the velocity comes out to be

$$\mathbf{v}_S^{\text{RP}} = \frac{(28l - 99\lambda)\lambda d_1 d_2 \omega \sin(\phi_1 - \phi_2)}{24l^2(4l - 17\lambda)} \hat{\mathbf{x}}, \quad (4.24)$$

again for equal reduced friction coefficients $\lambda_i = \lambda$ of the beads and equal mean lengths $l_i = l$ of the two arms of the swimmer, and where the superscript ‘RP’ again marks the use of the Rotne–Prager matrix instead of the Oseen tensor (here in the stroke-based calculation).

We observe that the velocity expressions in equations (4.23) and (4.24) reduce to those in equations (4.3) and (4.2), respectively, when only the lowest order terms in λ/l are kept in the numerator and the denominator, as they should. We also note that the difference between the two velocity expressions in the stroke-based formulation is only of a geometric factor at the beginning of the expression, which is not the case for the two velocity expressions obtained from the force-based formulation.

We can compare the four theoretical velocity formulae obtained for our swimmer, namely by using the force-centric and the stroke-centric approaches to two different orders in the hydrodynamic interactions. Figure 2 shows such a comparison for a swimmer with a varying l/λ ratio. As expected, the four velocity expressions converge to the same curve as the l/λ ratio becomes larger.

4.2. Validation of simulations

For validation of the simulation system, we perform simulations of an isolated bead-spring swimmer and compare them with the theoretical expressions described in sections 4 and 4.1. The beads are spherical with a radius of $\lambda = 4$ cells and separated by mean distances of $l = 20$ cells. The fluid has a dynamic viscosity (on the lattice) of $\eta = 1/3$ (which also equals its kinematic viscosity ν defined as $\nu = \eta/\rho$, since the density of the fluid ρ is taken to be 1 on the lattice). The relaxation time is set to $\tau = 1.5$, and the spring stiffness (on the lattice) to $k = 0.0347$. The simulations are carried out in a box of size $(x \times y \times z) = (1200 \times 800 \times 800)$ lattice cells with

free-slip boundary conditions specified at the walls of the box. We perform six full swimming cycles in total to ensure that the steady state is reached. The other parameters in the different simulations are detailed in table 1 in the supplementary information (S.I.) (stacks.iop.org/JPhysCM/29/124001/mmedia). All the simulations are performed using the Emmy cluster of the RRZE computing centre in Erlangen [47].

Figure 3(a) shows the cycle-averaged velocity of the swimmer as a function of the cycle period, from simulations (dashed black line) and from theory, with the dashed-dotted red line marking the lower-order theory (with respect to the inter-bead hydrodynamic interactions) and the solid green line the higher-order one. We find that the simulation results compare very well to the theoretical curves, except at small cycle periods. The relative error between the simulations and the lower order theory (figure 3(b), dashed dotted red curve) go down continuously and for cycle periods larger than 4800 time steps become 10% or smaller, becoming nearly 0% for a cycle period of 10 000 time steps. It is simple to understand why the simulations perform better as the cycle period increases. Firstly, the smaller the cycle period is, the larger are the errors due to time discretization. Secondly, small time periods result in larger instantaneous bead Reynolds numbers (these becoming, for instance, larger than 0.2 in the simulation with a cycle period of 1000 time steps).

When we compare the simulations with the higher order theory, we find that the relative error (shown as a solid green curve in figure 3(b)) again initially decreases with the cycle period, but for cycle periods larger than 4000 time steps it becomes stable at about 8%. This is within the expected error range of 5%–10% in lattice Boltzmann simulations due to the presence of the simulation walls, time and space discretization errors, and other numerical artefacts. As the cycle period increases to 10 000 time steps, the errors with respect to the lower order theory are even smaller than that for the higher order one, and this is likely due to a fortuitous cancellation. In either case, they remain below 10%.

Apart from the swimming velocity, we also check the dependence of the stroke parameters on the driving force amplitude ratio A/B (in figure 3(c)) and on the force phase shift α (figure 3(d)). For this we use the relatively small cycle period of 4800 time steps in the simulations (where, from figures 3(a) and (b), the errors in the velocity with respect to both the first and the second order theories go down to 10%). In both the cases, the expected stroke parameters are reproduced very well in the simulations.

5. Swarms of swimmers

Understanding the motion of a single swimmer is a prerequisite for studying the behavior of swarms, which are large populations of individuals whose trajectories are coordinated and interdependent in complex ways. Here we present swarm simulations, comprised of thousands of individual swimmers. In the literature, the swimmers within a swarm are not usually represented individually as doing so is often prohibitively expensive computationally. If possible, however, such

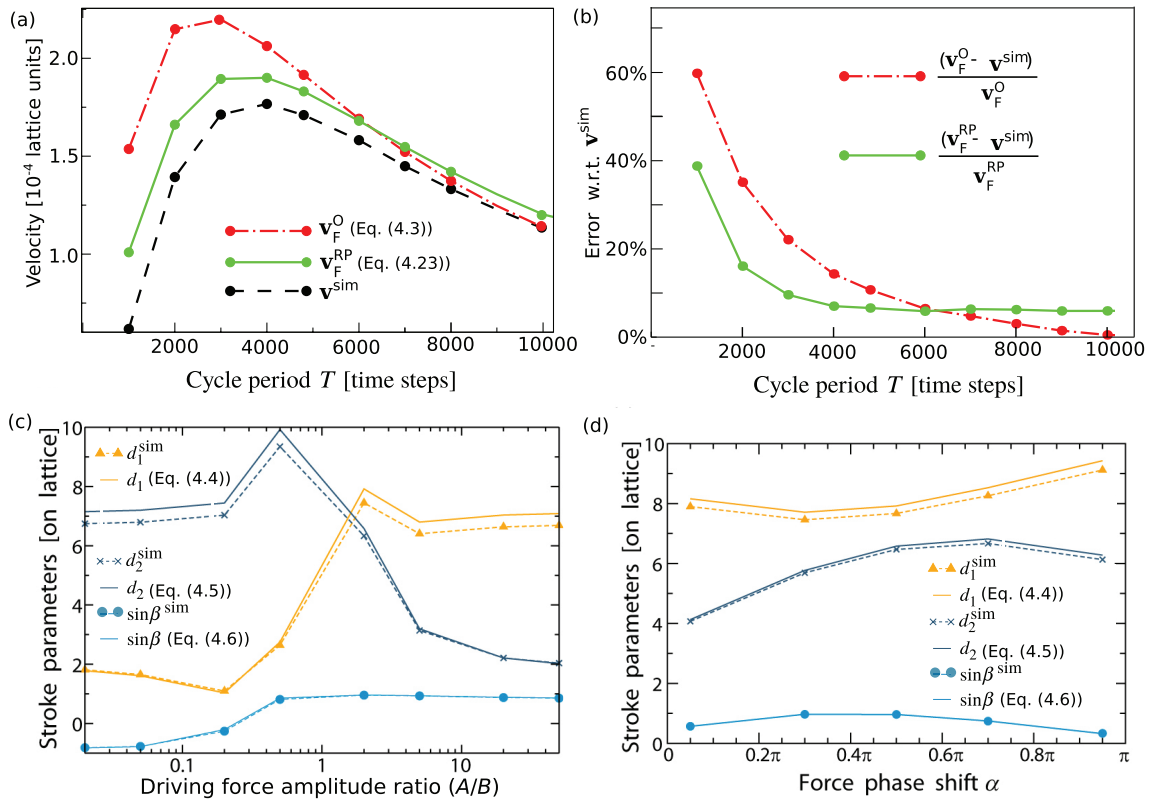


Figure 3. (a) Comparison of the cycle-averaged swimming velocity from simulations and from theory for two different orders in sphere radius-to-separation ratio, for different cycle periods. (b) Relative error between the velocities from simulations and from the two theoretical expressions in equations (4.3) and (4.23). (c) and (d) The dependence of the stroke parameters on the force amplitude ratio A/B and the force phase shift α , respectively, for a simulation with cycle period 4800 time steps. The superscript ‘sim’ denotes simulation results.

a fine-grained approach can shed important light on how the interactions amongst individuals executing simple motion result in the rich cooperative behavior that swarms typically exhibit. We therefore adopt the latter, fully-detailed approach.

In our simulations we use between 60 and 1280 compute cores, and place $1 \times 3 \times 3$ swimmers on each core, so that there are up to 11520 swimmers in our swarms. Our approach is to begin with smaller swarms of 540 swimmers (on 60 cores), and, if these result in simulations that run successfully, to scale them up to 11520 swimmers. The distances between the swimmers on one core are C_y and C_z along the y - and z -directions, respectively, and within two neighboring swimmers on *different* cores are D_x , D_y and D_z along the three axes (figure 4). The entire configuration is always kept symmetric along the y - and z -directions, so that $C_y = C_z$ and $D_y = D_z$. Periodic boundary conditions are imposed at the walls of the simulation box.

The individual swimmers within each swarm are composed of spherical beads with a radius of $\lambda = 6$ cells and separated by a mean distance of $l = 32$ cells. The driving force amplitude is 2, and the force phase shift is 0.5π . The cycle period is kept at 2000 time steps, since this value serves the dual purposes of enabling the individual swimmer velocity to be relatively high while keeping the cycle period small (see figure 3(a)). Both of these features are important in allowing the inter-swimmer interactions within large swarms

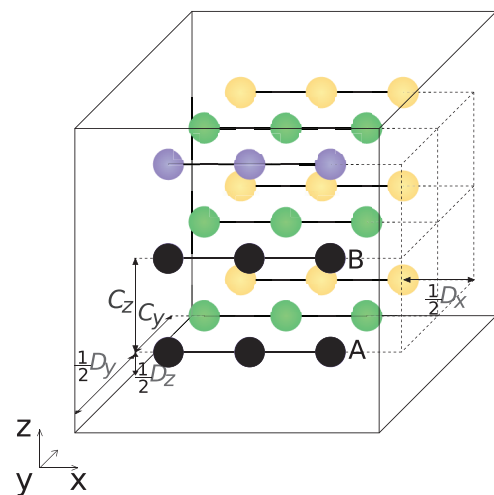


Figure 4. Setup of the swarm simulation on each core for both uniform and non-uniform initial arrangements of the swimmers within a swarm. The distances between the swimmers within one core are C_y and C_z along the y - and z -directions, respectively, and within two neighboring swimmers on different cores are D_x , D_y and D_z along the three axes. Two particular swimmers A and B are marked for later comparison of trajectories.

to propagate quickly. The simulations are run for up to 124 swimming cycles. In any simulation, if the instantaneous swimming velocity exceeds 0.5 lattice cell/time step, then

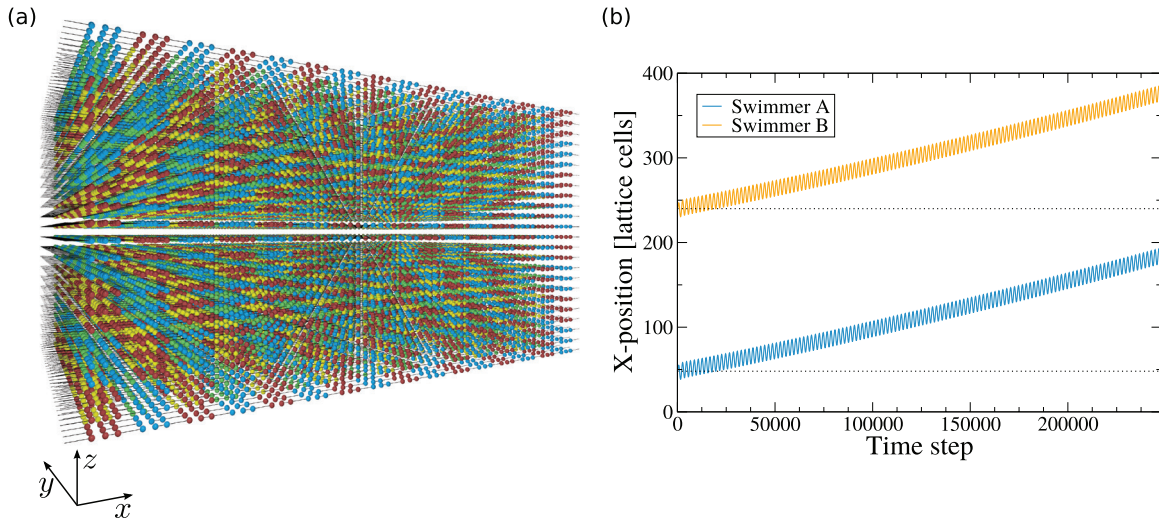


Figure 5. (a) The configuration of a stably moving swarm at the end of 124 swimming cycles. The colors group together the beads which are being handled by one process at the particular instant considered. In each direction the colors are arranged in a checkerboard pattern. (b) The x -trajectories of the middle beads of two selected swimmers within the swarm.

the simulation is terminated. This is because, firstly, such a velocity results in Reynolds numbers larger than 10 which is much beyond the typical values in microswimming, and secondly, traversal of more than half a cell length in a time step by a bead can result in an incorrect exchange of momentum between different lattice cells in the simulations.

We have simulated various configurations, listed in table 2 in the S.I., where the initial inter-swimmer distances ($C_y = C_z, D_x, D_y = D_z$) vary. In the first setup we study (simulations (a) and (b) in table 2 in the S.I.), the swimmers are arranged initially on a regular cubic lattice, with the distances between any two neighboring swimmers in any direction ($C_y = C_z = D_x = D_y = D_z$) being 32 lattice units. We find that such an initial configuration results in a steady motion of the swarm along the x -axis over the course of the simulation. This setup can be identified as a non-equilibrium steady state. Figure 5(a) shows the configuration of the swarm at the end of 124 swimming cycles. The regularity in the arrangement of the swarm can be easily seen, and is also illustrated by the x -coordinates of two randomly-chosen swimmers within the swarm shown in figure 5(b), which exhibit a uniform cycle-averaged velocity. Which two swimmers are chosen is immaterial, since the configuration is stable and the local neighborhood of each swimmer remains identical throughout the simulation. The y - and z -positions of all the swimmers are constant over the entire simulation time.

We now disturb the steady state by introducing spacing defects in the initial arrangement of the swarm. For this we keep $C_y \neq D_y$ (and consequently $C_z \neq D_z$), which means that the swarm is split into layers along both the y - and the z -directions, with the swimmers within each layer being equidistant (but with this distance being unequal to the separation between the different layers). We find that most of these defects induce strong hydrodynamic forces acting asymmetrically between the swimmers, which cause them to accelerate to high swimming speeds (larger than 0.5 lattice cell/time step) such that they cannot be appropriately

resolved in the simulations, and the simulations consequently terminate.

However, one particular setup (simulations (c) to (g) in table 2 in the S.I.) demonstrates transiently oscillating behavior along the axis of driving (the x -axis) over the course of the simulation time. Here we have $C_y = C_z = 37, D_x = 56$ and $D_y = D_z = 46$ lattice units. The two representative swimmers A and B (marked in figure 4) show identical motion along the x -direction (figure 6), indicating that the entire swarm oscillates coherently along the axis of driving.

In the other two directions, the local environment of a swimmer affects its motion. There are two significant differences in the initial placement of swimmers A and B within the swarm (figure 4). Firstly, the y and z directions are identical for swimmer A but not for swimmer B. Secondly, the whole swarm is symmetric around swimmer B along the z -axis but not along the y -axis (since swimmer B is the middle swimmer in its core in the z -direction but not in the y -direction), while for swimmer A the swarm is symmetrically placed neither along the z - nor the y -axis (if $C_z \neq D_z$ and $C_y \neq D_y$). Due to this, the two swimmers face different hydrodynamic forces from the other swimmers in the swarm and consequently execute dissimilar motion along different directions. Swimmer A undergoes a rotation in the x - z plane (demonstrated by the z -trajectories of its three spheres in figure 6(b)), which, due to its z -symmetry, is absent in the case of swimmer B (within an error of one lattice cell, not shown here). The rotation of swimmer A in the x - y plane is, as expected, identical to that in the x - z plane (not shown). In contrast, swimmer B undergoes significant rotation only in the x - y plane (figure 6(c)). Moreover, swimmer B changes its orientation with respect to the x -axis only once during the simulation time, unlike swimmer A which does so twice. For this swarm we see that the swimmers display cooperative behavior, by moving as one along the axis of driving (the x -axis), yet differences in their motion are equally visible, as evidenced by the different kinds of rotation observed for different swimmers. It remains unclear how much of the cooperation between the swimmers derives from the identical driving forces which

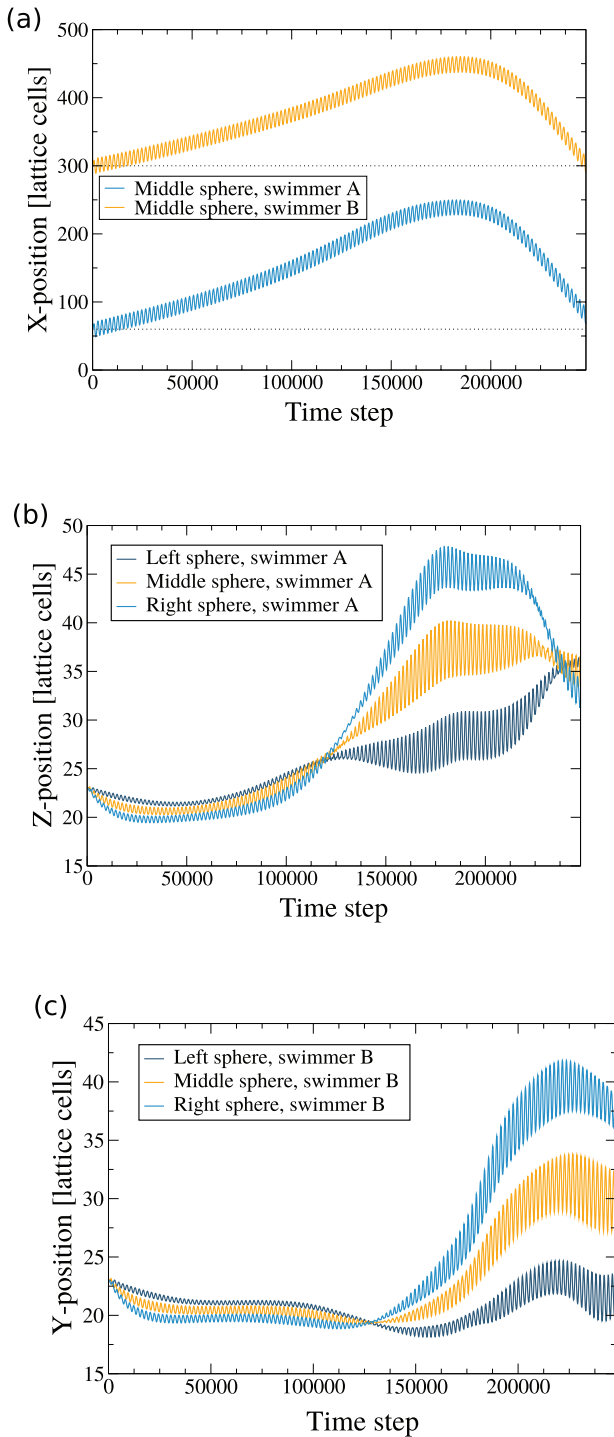


Figure 6. (a) Trajectories along the x -direction of the middle spheres of swimmers A and B marked in figure 4, indicating that the entire swarm oscillates along the x -direction. (b) Trajectories along the z -direction of the three spheres of swimmer A, showing the rotation of the swimmer in the x - z plane. (c) Trajectories along the y -direction of the three spheres of swimmer B, showing the rotation of the swimmer in the x - y plane.

all the swimmers are subjected to, and to what extent the boundary conditions affect this behavior. In any case, our simulations show that large swarms of microswimmers are by and large unstable under the condition of fixed driving. An important consequence, for both artificial microswimmer swarms as well as biological ones such as those formed by bacteria, is

that in order to maintain order in a swarm, some kind of self-regulation in the stroke of the individual swimmers is essential, as otherwise the hydrodynamic forces result in the breaking up of the swarm.

6. Summary and conclusion

Here we have expanded upon our previous study of the bead-spring swimmer model wherein we analyse its motion starting from a description of the driving forces [21, 48]. In this paper we have extended the accuracy of our prior calculations by including higher order terms in the hydrodynamic interactions between the beads in the swimmer. Along with the theory, we have here studied the motion of the swimmer numerically using the WALBERLA-*pe* simulation system based on the lattice Boltzmann method. The accuracy of the simulations is verified by good agreement with the theoretical expressions to both investigated orders in the hydrodynamic interactions, which gets better as the cycle period increases due to better time discretization and reduced Reynolds numbers. Comparison with the higher order theory shows that the simulation errors saturate to a value below 10% for cycle periods larger than 4000 time steps.

After studying single swimmers, we have simulated swarms containing thousands of individuals. We have shown that a particular uniform spacing between the different swimmers in the swarm results in a stable uniaxial motion. Introducing defects in the uniformity of the swarm results in differences emerging in the motion of individual swimmers within the swarm. For one particular initial swarm spacing (with unequal separation distances along the three axes), some swimmers show a pronounced rotation along different axes, but along the axis of driving the swarm oscillates as one body. The differences in the responses of individual swimmers are due to the unequal hydrodynamic forces that they face from other swimmers in the swarm, the effect of which builds up over the simulation time. For all the other initial separation distances tried, the simulations terminate due to strong acceleration of the swimmers caused by their hydrodynamic interaction. It is here worthwhile to note that unlike in the swarm case, an isolated swimmer with the same parameters and facing the same driving forces swims within the Stokes regime (at Reynolds numbers smaller than 1).

Our results speak to the instabilities which grow rapidly and result in a complete breaking of the initial order in the swarms when their members are allowed to respond individually to the different forces upon the system. With this in mind, it would be interesting to implement a few extensions to the simulation methodology. In the present simulations, all the swimmers act under an identical force protocol, as would be the case if an artificial swarm is propelled by an oscillating external field. A different kind of swarm behavior could occur if each swimmer within the swarm is associated with a (slightly) different driving protocol, as for instance is the case in living systems. The sensitivity of the stable phase points to the fact that in living systems the stroke must be adjusted by regulating the energy invested

into forcing the different body parts of a swimmer, in order to maintain the stability of the swarm. If the hydrodynamic interactions are amplified to such an extent that they cannot be compensated by the self-regulation of the swimmers, then the swarm should become unstable (as in most of the simulated cases here). However, our results show that even if the stroke of the swimmers is not identical (such as due to the introduced spacing defects in our simulations) and not self-correcting, some synchronization between the swimmers can take place in a passive manner. It remains to be clarified whether this synchronization is a result of experiencing an identical driving protocol, or is dominated by hydrodynamic interactions.

In order to improve the accuracy of the simulations, second order boundary conditions could be implemented at the swimmer-fluid interfaces, and an adaptive mesh refinement could be employed which would reduce computational cost. This would permit longer simulations, which are at the moment not possible due to limited availability of the supercomputing resources. However, even with the current limitations, we have been able to build up a fully resolved microswimming model and to expand it to the simulation of large swarms composed of thousands of instances of the same fully-resolved swimmer. Such a level of detail is, to our knowledge, unique for a swarm and is a promising harbinger of more insight into the complex patterns displayed by real swarms, the members of which, at a fundamental level, are individual entities navigating their immediate environments.

Acknowledgments

This work was supported by the Kompetenznetzwerk für Technisch-Wissenschaftliches Hoch- und Höchstleistungsrechnen in Bayern (KONWIHR) under the ParSwarm project, and by the Cluster of Excellence: Engineering of Advanced Materials at the Friedrich-Alexander University Erlangen-Nürnberg.

Appendix

Here we show how to obtain the expression for \mathbf{v}_i , the velocity of the i th bead, in (4.13) in the calculation of the Rotne–Prager matrix for beads with unequal reduced friction coefficients λ_i .

From equations (4.10)–(4.12), we get

$$\mathbf{v}_i = \frac{-1}{6\pi\eta\lambda_i} \mathbf{F}_i^h + \left(\frac{-1}{6\pi\eta\lambda_j} \right) \left(1 + \frac{1}{6} \lambda_i^2 \nabla^2 \right) \left\{ \left[\frac{3}{4} \left(\frac{\lambda_j}{r_{ij}} \right) (\mathbb{I} + \hat{\mathbf{r}}_{ij} \hat{\mathbf{r}}_{ij}) + \frac{1}{4} \left(\frac{\lambda_j}{r_{ij}} \right)^3 (\mathbb{I} - 3\hat{\mathbf{r}}_{ij} \hat{\mathbf{r}}_{ij}) \right] \cdot \mathbf{F}_j^h \right\}. \quad (\text{A.1})$$

To simplify the above expression, we note that in spherical polar coordinates we have

$$\nabla^2 \left(\frac{1}{r^3} \right) = 6r^{-5}, \quad (\text{A.2})$$

$$\nabla^2 \left(\frac{1}{r} \right) = 0, \text{ for } r \neq 0, \quad (\text{A.3})$$

$$\nabla_i^2 \left\{ \frac{1}{r_{ij}} [\mathbb{I} + \hat{\mathbf{r}}_{ij} \hat{\mathbf{r}}_{ij}] \right\} = 2 \left(\frac{1}{r_{ij}} \right)^3 [\mathbb{I} - 3\hat{\mathbf{r}}_{ij} \hat{\mathbf{r}}_{ij}], \text{ and} \quad (\text{A.4})$$

$$\nabla_i^2 \left\{ \left(\frac{1}{r_{ij}} \right)^3 [\mathbb{I} - 3\hat{\mathbf{r}}_{ij} \hat{\mathbf{r}}_{ij}] \right\} = 0. \quad (\text{A.5})$$

Using equations (A.1)–(A.5), we can write the second-order velocities as

$$\mathbf{v}_i = \frac{-1}{6\pi\eta\lambda_i} \mathbf{F}_i^h + \sum_{j \neq i} \left(\frac{-1}{6\pi\eta\lambda_j} \right) \left[\frac{3}{4} \left(\frac{\lambda_j}{r_{ij}} \right) (\mathbb{I} + \hat{\mathbf{r}}_{ij} \hat{\mathbf{r}}_{ij}) + \frac{1}{4} \left(\frac{\lambda_j}{r_{ij}} \right)^3 (\mathbb{I} - 3\hat{\mathbf{r}}_{ij} \hat{\mathbf{r}}_{ij}) \right] \cdot \mathbf{F}_j^h - \sum_{j \neq i} \frac{1}{36\pi\eta\lambda_j} \lambda_j^2 \left\{ \frac{3}{4} \lambda_j \left[2 \left(\frac{1}{r_{ij}^3} \right) (\mathbb{I} - 3\hat{\mathbf{r}}_{ij} \hat{\mathbf{r}}_{ij}) + \frac{1}{4} \left(\frac{\lambda_j}{r_{ij}} \right)^3 (0) \right] \right\} \cdot \mathbf{F}_j^h. \quad (\text{A.6})$$

Collecting like terms leads to (4.13).

References

- [1] Lauga E and Powers T R 2009 *Rep. Prog. Phys.* **72** 096601
- [2] Elgeti J, Winkler R G and Gompper G 2015 *Rep. Prog. Phys.* **78** 056601
- [3] Copeland M F and Weibel D B 2009 *Soft Matter* **5** 1174
- [4] Pedley T J, Hill N A and Kessler J O 1988 *J. Fluid Mech.* **195** 223
- [5] Ghorai S and Hill N A 1999 *J. Fluid Mech.* **400** 1
- [6] Riedel I H, Kruse K and Howard J 2005 *Science* **309** 300
- [7] Guehl D C, Brenner H, Frankel R B and Hartman H 1988 *J. Theor. Biol.* **135** 525
- [8] Carlile M J and Dudeney A W L 1993 *J. Gen. Microbiol.* **139** 1671
- [9] Drescher K, Leptos K C, Tuval I, Ishikawa T, Pedley T J and Goldstein R E 2009 *Phys. Rev. Lett.* **102** 168101
- [10] Taylor G 1951 *Proc. R. Soc. A* **209** 447
- [11] Lighthill M J 1952 *Commun. Pure Appl. Math.* **5** 109
- [12] Blake J R 1971 *J. Fluid Mech.* **46** 199
- [13] Avron J E, Kenneth O and Oaknin D H 2005 *New J. Phys.* **7** 234
- [14] Pooley C M, Alexander G P and Yeomans J M 2007 *Phys. Rev. Lett.* **99** 228103
- [15] Najafi A and Golestanian R 2004 *Phys. Rev. E* **69** 062901
- [16] Ledesma-Aguilar R, Löwen H and Yeomans J M 2012 *Eur. Phys. J. E* **35** 70
- [17] Drescher K, Goldstein R E, Michel N, Polin M and Tuval I 2010 *Phys. Rev. Lett.* **105** 168101
- [18] Friedrich B M and Jülicher F 2012 *Phys. Rev. Lett.* **109** 138102
- [19] Felderhof B U 2015 *Phys. Rev. E* **92** 063014
- [20] Felderhof B U 2006 *Phys. Fluids* **18** 063101
- [21] Pande J and Smith A S 2015 *Soft Matter* **11** 2364–71
- [22] Feichtinger C, Donath S, Köstler H, Götz J and Rüde U 2011 *J. Comput. Sci.* **2** 105–12
- [23] Pickl K, Hofmann M, Preclik T, Köstler H, Smith A S and Rüde U 2014 *Parallel Computing: Accelerating Computational Science and Engineering (Advances in Parallel Computing vol 25)* (Amsterdam: IOS Press) pp 395–404
- [24] Aranson I S, Sokolov A, Kessler J O and Goldstein R E 2007 *Phys. Rev. E* **75** 040901
- [25] Wolgemuth C W 2008 *Biophys. J* **95** 1564

- [26] Wensink H H, Dunkel J, Heidenreich S, Drescher K, Goldstein R E, Löwen H and Yeomans J M 2012 *Proc. Natl Acad. Sci. USA* **109** 14308
- [27] Oyama N, Molina J J and Yamamoto R 2016 *Phys. Rev. E* **93** 043114
- [28] Purcell E M 1977 *Am. J. Phys.* **45** 3–11
- [29] Köstler H and Rüde U 2013 *IT—Inf. Technol.* **55** 91–6
- [30] Feichtinger C, Habich J, Köstler H, Hager G, Rüde U and Wellein G 2011 *Parallel Comput.* **37** 536–49
- [31] Iglberger K and Rüde U 2011 *Multibody Syst. Dyn.* **25** 81–95
- [32] Qian Y H, d’Humières D and Lallemand P 1992 *Europhys. Lett.* **17** 479–84
- [33] Ginzburg I, Verhaeghe F and d’Humières D 2008 *Commun. Comput. Phys.* **3** 427–78
- [34] Godenschwager C, Schornbaum F, Bauer M, Köstler H and Rüde U 2013 *Proc. Int. Conf. on High Performance Computing, Networking, Storage, and Analysis (ACM)* pp 35:1–12
- [35] Pickl K, Götz J, Iglberger K, Pande J, Mecke K, Smith A S and Rüde U 2012 *J. Comput. Sci.* **3** 374–87
- [36] Götz J, Iglberger K, Stürmer M and Rüde U 2010 *Proc. 2010 ACM/IEEE Int. Conf. for High Performance Computing, Networking, Storage and Analysis* (IEEE Computer Society) pp 1–11
- [37] Ladd A J C 1994 *J. Fluid Mech.* **271** 285–309
- [38] Ladd A J C 1994 *J. Fluid Mech.* **271** 311–39
- [39] Yu D, Mei R, Luo L S and Shyy W 2003 *Prog. Aerosp. Sci.* **39** 329–67
- [40] Iglberger K, Thürey N and Rüde U 2008 *Comput. Math. Appl.* **55** 1461–8
- [41] Golestanian R and Ajdari A 2008 *Phys. Rev. E* **77** 036308
- [42] Oseen C W 1927 *Neuere Methoden und Ergebnisse in der Hydrodynamik* (Leipzig: Akademische Verlagsgesellschaft)
- [43] Rotne J and Prager S 1969 *J. Chem. Phys.* **50** 4831
- [44] Aguirre J L and Murphy T J 1973 *J. Chem. Phys.* **59** 1833
- [45] Dhont J K G 1996 *An Introduction to Dynamics of Colloids* (Amsterdam: Elsevier)
- [46] Faxén H 1922 *Ann. Phys.* **373** 89
- [47] EMMY information on the EMMY cluster www.rze.fau.de/dienste/arbeiten-rechnen/hpc/systeme/emmy-cluster.shtml
- [48] Pande J, Merchant L, Krüger T, Harting J and Smith A S 2014 arXiv:1411.5723